15 September 2002

ELSEVIER

Optics Communications 210 (2002) 393–398

OPTICS COMMUNICATIONS

www.elsevier.com/locate/optcom

Efficient second, third, fourth, and fifth harmonic generation of a Yb-doped fiber amplifier

Dahv A.V. Kliner[a,*], Fabio Di Teodoro[b], Jeffrey P. Koplow[b], Sean W. Moore[b], Arlee V. Smith[c]

[a] *Sandia National Laboratories, Combustion Research Facility, P.O. Box 969, MS 9056, Livermore, CA 94551, USA*
[b] *Naval Research Laboratory, Washington, DC 20375, USA*
[c] *Sandia National Laboratories, Albuquerque, NM 87185, USA*

Received 30 May 2002; received in revised form 30 July 2002; accepted 31 July 2002

Abstract

We report generation of the second, third, fourth, and fifth harmonics of the output of a Yb-doped fiber amplifier seeded by a passively *Q*-switched Nd:YAG microchip laser. We obtained high conversion efficiencies using a simple optical arrangement and critically phase-matched nonlinear crystals. Starting with 320 mW of average power at 1064 nm (86 μJ per pulse at a 3.7 kHz repetition rate), we generated 160 mW at 532 nm, 38 mW at 355 nm, 69 mW at 266 nm, and 18 mW at 213 nm. The experimental results are in excellent agreement with calculations.

PACS: 42.65.Ky; 42.72.Bj; 42.55.Wd; 42.81.-i

Keywords: Ultraviolet generation; Optical fiber amplifiers; Frequency conversion; Ytterbium

1. Introduction

Compact and efficient sources of visible and ultraviolet (UV) radiation are required for a wide range of applications. In many cases, continuous tunability, broad wavelength coverage, narrow linewidth, high peak or average power, and high beam quality are also needed. Frequency conversion of pulsed, rare-earth-doped fiber lasers and amplifiers offers the possibility of a practical source that meets all of these requirements [1–6]. Fiber-based systems have not been widely used for visible and UV generation, however, because of their relatively low pulse energies and peak powers (in comparison to bulk lasers) and consequent low nonlinear conversion efficiency. In the past several years, techniques have been developed for significantly increasing the pulse energy and peak power of fiber sources [7–12], opening up the possibility of efficient nonlinear frequency conversion throughout the visible and UV spectral regions using standard nonlinear crystals. In this paper, we report generation of the second, third, fourth, and

* Corresponding author. Tel.: +19252942821; fax: +19252942595.
E-mail address: dakline@ca.sandia.gov (D.A.V. Kliner).

0030-4018/02/$ - see front matter
PII: S0030-4018(02)01825-4

fifth harmonics of a high-pulse-energy, Yb-doped, double-clad (DC) fiber amplifier seeded by a pulsed Nd:YAG microchip laser.

2. Experimental setup

Fig. 1 shows a schematic diagram of the apparatus. The fiber amplifier was similar to that described in [12]. In this system, high pulse energies and peak powers were enabled by the use of multimode gain fiber, but diffraction-limited beam quality was obtained by coiling of the fiber to suppress propagation of transverse modes other than the fundamental mode (LP_{01}) [13]. Specifically, the Yb-doped fiber had a core diameter and numerical aperture of 25 μm and ~0.10, respectively, which corresponds to a V-number of ~7.4 and a measured LP_{01} mode-field diameter of 19.5 μm at 1064 nm. For bend-loss-induced mode filtering, the fiber was coiled on two orthogonal spools of 1.67 cm diameter. The DC fiber was pumped near one end using the 976 nm cw output of a formatted diode bar (Limo), which provided up to 17 W of launched pump power (although <3 W was used for the present experiment). We used the technique of embedded-mirror side pumping, in which a mirror is embedded in a channel polished into the inner cladding of the DC fiber, and pump light is launched by reflection from the mirror [14].

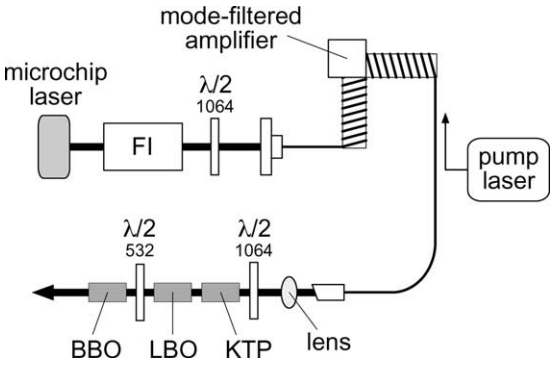

Fig. 1. Schematic diagram of the experimental apparatus. FI = Faraday isolator, $\lambda/2$ = half-wave plate (at the indicated wavelength in nm). Bold lines indicate free-space beams. The crystals used for fifth-harmonic generation are shown.

We used a different seed laser than that described in [12]. For the present experiment, the fiber amplifier was seeded with the 1064 nm output of a passively Q-switched Nd:YAG microchip laser (Poly-Scientific), which was pumped by an 808 nm diode laser. The seed laser produced transform-limited pulses with a nearly Gaussian temporal profile (0.97 ns FWHM) and an energy of ~10 μJ at a repetition rate of 3.5–3.9 kHz. The seed laser was optically isolated from the amplifier and was coupled into a single-mode fiber, which was fusion spliced to the Yb-doped fiber. The seed and pump beams were counter-propagating. The output end of the DC fiber was mode-stripped to remove light propagating in the inner cladding (similarly, the seed end of the amplifier was mode-stripped by the single-mode pigtail). The input and output facets were fusion spliced to fused-silica beam expanders to prevent optical damage, and both ends were angle-polished at 8° to eliminate feedback. The amplifier produced diffraction-limited output pulses with a temporal profile identical to that of the seed laser [12]. Half-wave plates were used to adjust the polarization of the seed beam and the amplifier output in order to provide linearly polarized light of the correct orientation for the nonlinear crystals.

The amplifier output beam was imaged using an $f = 11$ mm aspheric lens (Geltech) to a measured beam waist of ~360 μm ($1/e^2$ diameter). The nonlinear crystals were positioned near the beam waist and were angle tuned to maximize the conversion efficiency. In order to provide a compact, rugged, and simple setup, no lenses or other optics were placed between the crystals (other than a wave plate for generation of the fifth harmonic; see below). After passing through the crystal(s), the various harmonics were separated using a fused-silica Pellin–Broca prism, and the pulse energies were measured using either a pyroelectric detector (Molectron) or a biased, silicon photodiode (calibrated against the pyroelectric detector).

The second harmonic (532 nm) of the amplifier output was generated using Type II phase matching in a hydrothermally grown, 9-mm-long KTP crystal (XY cut, $\theta = 90°$, $\phi = 26°$; Poly-Scientific). The fourth harmonic (266 nm) was generated by Type I doubling of the 532 nm light in either a

BBO crystal (15 mm, 48°; Castech) or a KD*P crystal (20 mm, 88°; Cleveland Crystals). Alternatively, the third harmonic (355 nm) was generated by Type I mixing of the 532 nm radiation with the residual 1064 nm radiation of the same polarization using LBO (10 mm, XY, $\theta = 90°$, $\phi = 37°$; Castech). Finally, the fifth harmonic (213 nm) was generated by mixing the 532 and 355 nm radiation using Type I mixing in BBO (20 mm, 70°; Castech); a zero-order wave plate (full-wave at 355 nm, half-wave at 532 nm) was inserted between the LBO and BBO crystals to rotate the polarization of the 532 nm beam to be parallel to that of the 355 nm beam. All crystals and wave plates were anti-reflection coated for the appropriate wavelengths on the input and output faces (reflection losses of <0.2% per face).

3. Results and discussion

The results are summarized in Fig. 2, which shows the pulse energies (P_i, where i is the wavelength in nm) and corresponding average powers of the amplifier output and of the various harmonics as a function of current supplied to the pump diode. The measurements have been corrected for Fresnel losses on the Pellin–Broca prism (1.0–21%, depending on the wavelength and polarization state). At the highest current of 13.3 A, the pulse energies (average powers) were 86 μJ (320 mW) at 1064 nm, 43 μJ (160 mW) at 532 nm, 10 μJ (38 mW) at 355 nm, 19 μJ (69 mW) at 266 nm, and 4.7 μJ (18 mW) at 213 nm.

For peak powers above ~60 kW (P_{1064} above ~60 μJ), we observed polarization instability of the amplifier output caused by nonlinear birefringence [15,16], which resulted in a corresponding instability in the doubling efficiency. The threshold power for the onset of nonlinear birefringence corresponds to a polarization beat length of ~25 cm [15], a reasonable value for commercial fiber [17]. This effect would be eliminated by the use of polarization-maintaining DC fiber [18], allowing even higher peak powers [12] and conversion efficiencies to be obtained.

We have performed calculations using the SNLO computer program [19] to compare with the experimental results. This analysis took into account the spatial and temporal profiles of the

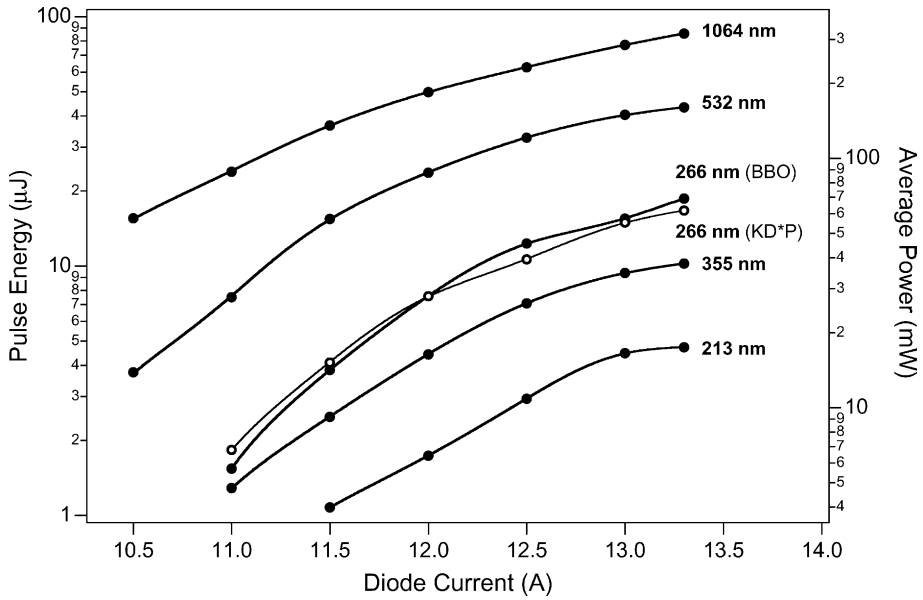

Fig. 2. Pulse energy and corresponding average power as a function of current supplied to the pump diode for the amplifier output (1064 nm) and for the indicated harmonics. The points are the experimental results, and the curves are smoothing splines.

beams, beam divergence (diffraction) and overlap, walk-off in each crystal, and losses between and within the crystals. We find very good agreement between the measurements and the calculations. Fig. 3a shows the measured and calculated P_{532} values as a function of P_{1064} incident on the KTP crystal. The dashed curve indicates the results of the calculation performed with no adjustable parameters (i.e., with the experimentally determined 1064 nm pulse energy, pulse duration, and beam waist); this calculation slightly over-predicts P_{532}. The solid curve shows the results of the calculation with the beam diameter increased by 15% (from 360 to 420 μm, i.e., within the uncertainty of the beam-waist measurement), which gives nearly perfect agreement with the experiment; the deviation of the measurements from the calculation for $P_{1064} > 60$ μJ was caused by the nonlinear polarization rotation discussed above. The maximum measured doubling efficiency was 52% (at $P_{1064} =$ 63 and 77 μJ).

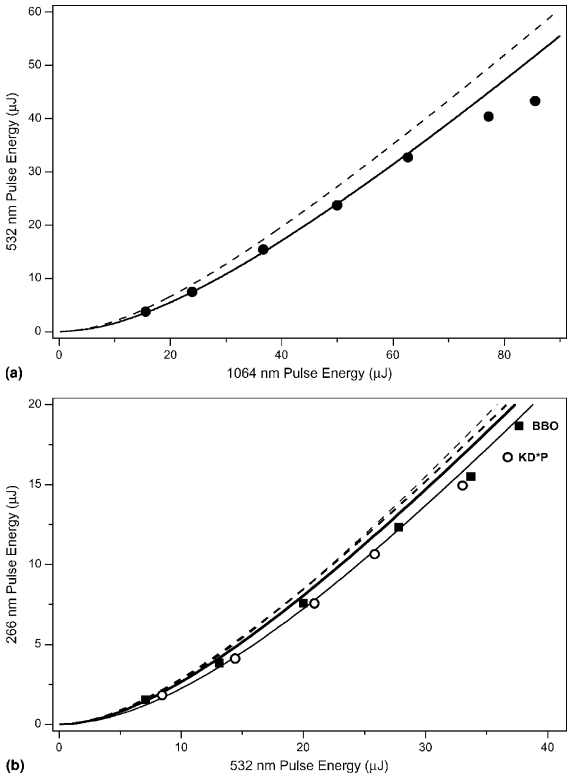

Fig. 3. (a) Generated 532 nm pulse energy versus 1064 nm pulse energy incident on the KTP crystal. The points are the experimental measurements; the curves are the results of the SNLO calculations, with the dashed (solid) curve corresponding to a 360 μm (420 μm) beam diameter. (b) Similar to (a), but showing the 266 nm pulse energy versus 532 nm pulse energy. The squares and bold curves correspond to BBO, and the circles and thin curves correspond to KD*P.

The highest value of P_{1064} corresponds to a peak fluence at the KTP crystal of 160 MW/cm^2. For peak fluences above ~200 MW/cm^2, we observed distortions of the 532 nm beam caused by photorefractive effects in the KTP crystal. The photorefractive threshold could be increased by maintaining the crystal at an elevated temperature [20], which would permit a smaller beam waist and thus a higher doubling efficiency.

Fig. 3b shows the measured and calculated P_{266} values as a function of P_{532} incident on the crystal for both BBO and KD*P. As in Fig. 3a, the calculated P_{266} values are slightly higher than the measurements, but expanding the beam waist used in the calculation by 15% brings the experimental and theoretical results into nearly perfect agreement. Note that both the experiment and the calculations show almost identical nonlinear conversion efficiencies for the BBO and KD*P crystals; the 266 nm beam quality is significantly higher when using KD*P, however, because the walk-off angle in BBO (85 mrad) is much larger than that in KD*P (2.6 mrad). The maximum doubling efficiency was 50% for BBO and 46% for KD*P.

Comparing the calculations and measurements for the third and fifth harmonics is less straightforward because: (1) We did not simultaneously measure all of the relevant input and output pulse energies. Rather, we measured the harmonic of interest and the residual P_{532}, and we used these measurements (along with the previously measured conversion efficiencies for the upstream crystals) to calculate the incident pulse energies at each diode current; and (2) Walk-off in a given crystal caused distortion and non-optimal spatial overlap of the beams being mixed in subsequent crystals, an effect that was treated only approximately in the calculations. Specifically, for generation of 355 nm, we used the SNLO-calculated spatial profiles of the 1064 and 532 nm beams

emerging from the KTP crystal to determine their overlap integral relative to "ideal" Gaussian beams; the P_{355} values calculated for overlapped Gaussian beams were decreased by this factor for comparison with the experimental results (the factor ranged from 0.58 to 0.84, primarily because of distortion of the 1064 nm beam). For generation of 213 nm, the dominant effect was displacement between 532 and 355 nm beams entering the BBO crystal; this displacement was calculated using SNLO to be ~110 μm (~70% of the calculated 355 nm FWHM beam diameter) and was measured using a CCD camera to be 69% of the 355 nm FWHM emerging from the LBO crystal. The displacement was perpendicular to the BBO walk-off direction, but SNLO treats displacement only in the walk-off direction; we therefore made the approximation of offsetting the 532 nm beam in the walk-off direction for the calculation of P_{213}. For comparison, we also performed SNLO calculations for the case of no displacement, and we note that the displacement could easily be eliminated using a dispersive optical element or dichroic mirrors.

Fig. 4 shows the measured and calculated values of P_{355} and P_{213} as a function of pump diode current. The agreement between the measurements and the calculations is excellent, and the calculated values of P_{355} and P_{213} are not strongly dependent on the beam waist. In addition, the calculations indicate that P_{213} would be increased by a factor of >2 by optimizing the spatial overlap of the 532 and 355 nm beams (Fig. 4, thin curves).

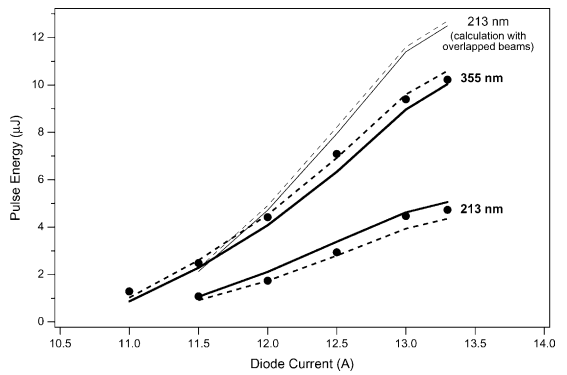

Fig. 4. Generated 355 and 213 nm pulse energies versus diode current. The points are the experimental measurements; the curves are the results of the SNLO calculations, with the dashed (solid) curves corresponding to a 360 μm (420 μm) beam diameter. The thin curves show the calculated P_{213} values with no offset between the 532 and 355 nm beams.

The seed laser and amplifier produced pulses with a transform-limited linewidth (~0.5 GHz). Although we did not measure the linewidth of the various harmonics, these pulses are also expected to be transform-limited because the acceptance bandwidths of the nonlinear crystals were 40–900 GHz and dispersion was negligible.

For the present experiment, the amplifier was operated well below its maximum power. At the highest current (13.3 A), the 1064 nm pulse energy, peak power, and average power were 86 μJ, 83 kW, and 320 mW, respectively; we have previously obtained 255 μJ, 305 kW, and 2.2 W with this amplifier (at a repetition rate of 8.5 kHz) [12]. Nonetheless, the nonlinear conversion efficiencies were very high because of the high peak power and the diffraction-limited beam quality produced by the mode-filtered amplifier. High conversion efficiencies can also be achieved by using noncritically phase-matched (temperature-tuned) or quasi-phase-matched crystals or by housing the crystals in resonant cavities, but these approaches increase the complexity and limit the tuning range of the system. The ability to use ambient-temperature, critically phase-matched crystals, single-pass mixing, and a simple optical setup (one lens) provides a compact, rugged approach to generation of radiation throughout the visible and UV spectral regions. The present results do not represent the maximum visible and UV powers attainable with fiber sources; by operating the laser system at higher repetition rates and pulse energies and by further optimizing the nonlinear conversion scheme, visible and UV powers of >1 W are possible.

Acknowledgements

This work was supported by Sandia's Laboratory Directed Research and Development Program and by the Air Force Philips Laboratory.

References

[1] J.P. Koplow, D.A.V. Kliner, L. Goldberg, IEEE Photon. Technol. Lett. 10 (1998) 75.
[2] D. Taverner, P. Briton, P.G.R. Smith, D.J. Richardson, G.W. Ross, D.C. Hanna, Opt. Lett. 23 (1998) 162.
[3] S.A. Guskov, S. Popov, S.V. Chernikov, J.R. Taylor, Electron. Lett. 34 (1998) 1419.
[4] S.V. Popov, S.V. Chernikov, J.R. Taylor, Opt. Commun. 174 (2000) 231.
[5] P.A. Champert, S.V. Popov, J.R. Taylor, J.P. Meyn, Opt. Lett. 25 (2000) 1252.
[6] G.J. Ray, T.N. Anderson, J.A. Caton, R.P. Lucht, T. Walther, Opt. Lett. 26 (2001) 1870.
[7] D. Taverner, D.J. Richardson, L. Dong, J.E. Caplen, K. Williams, R.V. Penty, Opt. Lett. 22 (1997) 378.
[8] J. Nilsson, R. Paschotta, J.E. Caplen, D.C. Hanna, Opt. Lett. 22 (1997) 1092.
[9] B.C. Dickinson, S.D. Jackson, T.A. King, Opt. Commun. 182 (2000) 199.
[10] C.C. Renaud, H.L. Oferhaus, J.A. Alvarez-Chavez, J. Milsson, W.A. Clarkson, P.W. Turner, D.J. Richardson, A.B. Grudinin, IEEE J. Quantum Electron. 37 (2001) 199.
[11] A. Galvanauskas, IEEE J. Select. Topics Quantum Electron. 7 (2001) 504.
[12] F. Di Teodoro, J.P. Koplow, S.W. Moore, D.A.V. Kliner, Opt. Lett. 27 (2002) 518.
[13] J.P. Koplow, D.A.V. Kliner, L. Goldberg, Opt. Lett. 25 (2000) 442.
[14] J.P. Koplow, S.W. Moore, D.A.V. Kliner, IEEE J. Quantum Electron. (2002), submitted.
[15] H.G. Winful, Opt. Lett. 11 (1986) 33.
[16] S.F. Feldman, D.A. Weinberger, H.G. Winiful, Opt. Lett. 15 (1990) 311.
[17] S.C. Rashleigh, IEEE J. Lightwave Technol. 1 (1983) 312.
[18] D.A.V. Kliner, J.P. Koplow, L. Goldberg, A.L.G. Carter, J.A. Digweed, Opt. Lett. 26 (2001) 184.
[19] A.V. Smith, D.J. Armstrong, W.J. Alford, J. Opt. Soc. Am. B15 (1998) 122, SNLO can be downloaded at no charge from http://www.sandia.gov/imrl/XWEB1 128/xxtal.htm.
[20] J.K. Tyminski, J. Appl. Phys. 70 (1991) 5570.